# Thermodynamic analysis of mono and hybrid nanofluid effect on the photovoltaic-thermal system performance: A comparative study

Mohammed Alktranee [a,b], Mohammed Ahmed Shehab [c,d,*], Zoltán Németh [e], Péter Bencs [a], Klara Hernadi [f]

[a] *Department of Fluid and Heat Engineering, Faculty of Mechanical Engineering and Informatics, University of Miskolc, Miskolc, HU-3515, Hungary*
[b] *Department of Mechanical Techniques, Technical Institute of Basra, Southern Technical University, Basrah, Iraq*
[c] *Faculty of Materials and Chemical Engineering, University of Miskolc, HU-3515, Miskolc, Hungary*
[d] *Polymers and Petrochemicals Engineering Department, Basrah University for Oil and Gas, Basrah, 61004, Iraq*
[e] *Advanced Materials and Intelligent Technologies Higher Education and Industrial Cooperation Centre, University of Miskolc, HU-3515, Miskolc, Hungary*
[f] *Institute of Physical Metallurgy, Metal Forming and Nanotechnology, University of Miskolc, H-3515, Miskolc, Hungary*

ARTICLE INFO

ABSTRACT

The energy and exergy efficiency of a photovoltaic thermal (PV/T) system at various volume fractions is investigated with mono $TiO_2$ nanofluid and new hybrid $TiO_2–Fe_2O_3$ nanofluid. Serpentine tubes soldered on an absorbing plate attached to the rear of the PV module have been proposed to evaluate the effect of nanofluids on the PV/T temperature reduction, energy produced, and exergy losses. The study compared energy and exergy with previous studies and delivered an economic analysis to confirm the feasibility of applying nanofluids. The results indicated that using $TiO_2–Fe_2O_3$ nanofluid reduced the PV cell's temperature by 42.19% compared to water, $TiO_2$ nanofluid, which increased the electrical power by 74.5% and 46.22% when cooling by mono and hybrid nanofluid at 0.3 vol%. The PV/T system's maximum thermal and electrical efficiency recorded with mono and hybrid nanofluids was 34.6%, 8.44%, 47.2%, and 12.62%, respectively. Dispersion of hybrid nanocomposite in DI water has enhanced the *Nu* number and HTC by 42.72% and 23% higher than mono nanofluid, which improved the exergy efficiency of the PV/T system by 14.89%. A better payback period was achieved with a hybrid nanofluid by 54 days with reduced exergy losses by 45.5% and entropy generation by 86.29%.

## 1. Introduction

In recent years, the energy sector has raised many concerns about the sustainability of energy supplies in future. This constitutes a huge burden on governments worldwide and a great incentive to adopt alternative sources to bridge the shortfall in energy supplies. Renewable energy is the most important alternative energy source for the future due to its high potential and reliable performance to compensate the shortfall in energy supply. Solar energy systems are effective and widespread due to their various applications to supply clean electrical and thermal energy without emissions which positively effects the environment. The solar industry is the best

## Nomenclature

| | |
|---|---|
| $A$ | PV/T area m$^2$ |
| $C_p$ | Specific heat kJ/kg. °C |
| $CuO$ | Copper Oxide |
| $S$ | Solar radiation W/m$^2$ |
| $I_{SC}$ | Short circuit current A |
| $I_{pv}$ | A current produced A |
| K | Thermal conductivity W/m·K |
| $Nu$ | Nusselt number |
| $HTC$ | Heat transfer coefficient W/m$^2$·K |
| $P_{pv}$ | Power produced W |
| $P_{inc}$ | Improvement percentage of electrical power % |
| $Q_u$ | Thermal energy W |
| $\dot{S} gen$ | Entropy generation W/°C |
| $T$ | Temperature °C |
| $V_{pv}$ | Voltage produced V |

*Subscript*

| | |
|---|---|
| amb | Ambient |
| DI | Deionised |
| FF | Fill Factor |
| bf | Base fluid |
| in | Input |
| np | Nanoparticles |
| out | Output |
| PV | Photovoltaic |
| $V_{OC}$ | Open circuit voltage |
| PV/T | Photovoltaic-thermal |

*Greek symbols*

| | |
|---|---|
| $\eta_{th}$ | Thermal efficiency of PV/T system % |
| $\eta_{ov}$ | Overall efficiency of PV/T system % |
| $\eta_{el}$ | Electrical efficiency % |
| $\rho$ | Density of fluid kg/m$^3$ |
| $\mu$ | Viscosity of fluid kg/ms |
| $\dot{E}x$ | Exergy W |
| $\eta_{\dot{E}_x}$ | Exergy efficiency of PV/T system % |
| $\varphi$ | Volume fraction% |
| $\dot{m}$ | mass flow rate L/min |

future energy option due to its availability, accessibility, cost-effectiveness, and efficiency compared to other renewable energies. Due to the increased demand for energy, the solar industry is rapidly developing worldwide because of the aggressive scientific research conducted to develop its performance, which became cost-effective applied [1]. Photovoltaic (PV) modules are a device that converts incident sunlight (solar radiation) into electricity [2]. The PV module made of semiconductor materials (typically silicon) consists of cells that convert short-wavelength solar radiation to electric energy [3]. The performance of the PV module is primarily dependent on the level of solar radiation it receives and the ambient temperature. Increasing the temperature of the PV cell leads to a decrease in conversion efficiency and a deterioration in the performance of the PV module [4]. The surface temperature of the PV module exhibits an inverse relationship with the electrical power of the PV module [5]. According to the findings, an increase in the temperature of the PV module by 1 °C leads to a drop in its efficiency by 0.45%–0.50% [6].

Furthermore, increasing the temperature of the PV cell lowers the output power, efficiency, and lifetime of the PV module [7]. Reducing the PV cell temperature is an important solution to maintain its performance, although it is difficult to achieve due to solar radiation and temperature fluctuations. Different cooling techniques have been applied to improve the performance of PV modules, including passive and active cooling, reducing the PV cell's temperature and increasing its efficiency [8]. Regarding passive cooling, different effective designs have been applied, such as (i) attaching phase change material (PCM) to the rear of the PV module for thermal management [9], (ii) placing different numbers and sizes of aluminium and copper fins at the rear of the PV module to increase the heat dissipation [10], and (iii) evaporative cooling using wet cotton wicks placed at rear of PV module [11]. In contrast, using active cooling methods significantly improves the PV module performance by adopting different cooling designs with the help of fluids that help reduce the PV cell's temperature and convert it to thermal energy. The PV/T system is an effective system consisting of a PV

module and a heat exchanger, characterised by high electrical power yield and electrical efficiencies resulting from circulating fluids at the rear of the PV/T system [12]. Indoor and outdoor experiments using mono and hybrid nanofluids at different volume fractions have been conducted to improve the efficiency of the PV/T system. In recently conducted research [13], a heat exchanger consisting of copper tubes was fixed on an aluminium plate placed at the rear of the PV module to reduce heat loss, whereas fibreglass was used to fill the pores. Compared with mono nanofluid, the outcomes indicated that using hybrid nanofluid $SiO_2$–$Al_2O_3$ at 0.5–0.5 wt had increased the thermal by 65.05% and electrical efficiencies by 13.17% for the outdoor experiment, while at the indoor experiment, the increment was by 65.08% and 11.47%, respectively. The results of the indoor and outdoor experiments demonstrate that the PV/T system's overall efficiency rose by 48.54% and 63.26% when cooled by pure water, while it climbed to 68.09% and 75.26% when cooled by a hybrid nanofluid of $SiO_2$–$Al_2O_3$. The results revealed that the hybrid nanofluid has a larger effect on the indoor experimental results than outdoor, and the difference in system efficiency between the two experiments has lowered from 14.72% to 7.17% when using a hybrid nanofluid. A numerical study verified by ANSYS Fluent was conducted using mono nanofluid CuO/water and hybrid nanofluid CuO–Fe/water (with a 50:50 mixing ratio) with inlet fluid velocity varied from 0.02 to 0.08 m/s to investigate the effect of two types of nanofluids on PV/T a system performance compared with cooling by water. A 3D geometry of the PV/T system represented by PV cells and tubes placed on an absorber plate was used to test the heat transfer mechanism by convection and conduction. The findings indicate that augmenting the velocity of the incoming fluid enhances thermal efficiency while having no impact on electrical efficiency.

In contrast, increased inlet fluid velocity had increased pressure drop. The maximum increment recorded for the thermal efficiency was 5.4% and electrical efficiency 2.14% for cooling with a hybrid nanofluid at 2 vol%. Conversely, mono nanofluid increases the efficiencies by 3.33% and 1.32% compared to the cooling by water, which emphasis the effectiveness of hybrid nanofluid [14]. Cobalt oxide ($CO_3O_4$/water) nanofluid and phase change material (PCM) mixed with $Al_2O_3$ nanopowder were experimentally studied as cooling methods for the PV/T-TEG system. Cooling the PV/T-TEG system by $Co_3O_4$/water nanofluid with 1 vol% increased the electrical power by 10.91% compared to water. The PV/T-TEG system's electrical efficiency has experienced a 4.52% enhancement with the utilization of both PCM and 1% nanofluid. Additionally, the exergy efficiency has seen an 11.6 rise in comparison to water cooling. The new configuration efficiently harnessed solar energy and improved the performance of the PV/T system compared to the reference PV module.

A mathematical model for the PV/T system derived from energy balance equations has been designed to study the effect of cooling by Cu/water and $Al_2O_3$/water to extract the excess heat from the PV cells and improve the performance of the PV/T system [15]. The numerical results of the proposed model have been validated by previous experimental studies. The results revealed a higher enhancement of the PV/T system efficiency by using Cu/water nanofluid than using $Al_2O_3$/water nanofluid due to the higher thermal conductivity of Cu nanoparticles. Compared with cooling by pure water, dispersing 2 vol% of Cu into a base fluid increased the electrical efficiency 1.9% and thermal efficiency by 4.1%, while using $Al_2O_3$ nanofluid has enhanced electrical and thermal efficiencies by 1.2% and 2.7%, respectively. An unglazed PV/T system performance has been evaluated by circulating water and CuO/water nanofluid into serpentine tubes placed on a thermal absorber plate and placed to the rear of the PV/T system [16]. The maximum temperature recorded at noon was 68.4 °C for the uncooled PV/T system, with an electrical efficiency of 12.98%. Cooling by water reduced the temperature to 15 °C then increased the electrical efficiency by 14.58% compared with an uncooled PV/T system. By using CuO nanofluid, the temperature of the PV cell was lowered to 23.7 °C, increasing the electrical efficiency by 35.67% and 20.78% compared to uncooled PV/T systems and water cooling. The PV/T system cooled with CuO nanofluid achieved a thermal efficiency of 71.17%, surpassing the 58.77% efficiency of the system cooled with water due to the superior heat absorption properties of CuO nanoparticles.

A PV/T system designed with a cooling system consisting of serpentine composite channels for water flow with microencapsulated PCM slurry placed in the space between the serpentine composite channels was studied experimentally by Fu et al. [17]. The electrical and thermal efficiencies have been compared using microencapsulated PCM slurry and water flow in various conditions. The experimental results showed a reduction in the PV cell temperature and an increment in electrical and thermal efficiency. The PV/T system performance was better when using microencapsulated PCM slurry than water with a PCM layer, in which the electrical and thermal efficiencies increased by 0.8% and 13.5%, respectively, confirming the feasibility of the applied cooling method. Using zirconium oxide ($ZrO_2$) nanofluid and DI water to lowering the PV cell's temperature was experimentally investigated under hot operation conditions [18]. Different volume fractions of $ZrO_2$ nanoparticles were dispersed in the host fluid circulated inside tubes soldered on an absorber plate and placed at the rear of the PV module. The results showed a remarkable reduction in the PV cell's temperature by up to 5.1 °C with the cooling by DI water and enhanced electrical power by 43.3% than the uncooled PV module. Cooling by $ZrO_2$ nanofluid at $\varphi = 0.0275$ vol% reduced the temperature to 10.2 °C compared to the uncooled PV module, the electrical power was improved by 93.3%, and the overall efficiency increased by 41.6%.

Three PV/T system configurations were used in an experimental investigation to examine the effects of mass flow rates (which ranged between 20 and 80 kg/h), varying volume fractions of water/magnetite nanofluid (0–2% vol%), and flow channel arrangement on the electrical efficiency of the PV/T systems [19]. The first configuration consisted of a sheet and serpentine tubes without fins (PV/T/0S), the second, there was a sheet and four serpentine tubes (PV/T/4S), and the third, there was a sheet and eight serpentine tubes (PV/T/8S). Their electrical efficiency was compared to a reference PV module without cooling. The PV/T system's maximum energy and exergy were reached at a flow rate of 80 kg/h and a volume fraction of 2%. The third configuration (i.e., PV/T/8S) provided higher overall efficiency by 5.87% and 15.59% than the PV/T/4S and PV/T/0S configurations, respectively. The maximum exergy efficiency recorded was 14.51% using PV/T/4S, and the electrical efficiency increment by 8.40%,10.87%, and 12.06% using configurations PV/T-0S, PV/T-4S and PV/T-8S, respectively. An experimental study using water/magnetite nanofluid as a cooling fluid circulating in two types of rifled serpentine tubes configurations (3 ribs and 6 ribs), which was used as a replacement for plain

serpentine, attached on an absorbed plate that placed at the rear of PV module. Nanofluid was circulated with different flow rates of 20–80 kg/h and volume fraction from 0 to 2% to compare rifled serpentine tube configurations used with conventional tubes to increase the energy and exergy of the PV/T system. The serpentine tube configuration with 6 ribs achieved overall energy and exergy efficiency of the PV/T system of 22.5%, 3.8%, 5.9%, and 1.9% higher than 3 ribs configuration at 2 vol% with a flow rate of 80 kg/h. Both rifled serpentine tube configurations achieved better performance than conventional tubes due to the increase in the heat transfer area and effective of nanofluid used cooling fluids than water [20].

In literature, experimental and numerical studies adopted different types of cooling designs and nanofluids, whether mono or hybrid nanofluids and achieved good outcomes and increased of the PV/T system efficiency. However, many studies lack a comprehensive analysis of the PV/T system performance, such as the quantity and quality performance of the PV/T system and economic feasibility and reliability of data measurement of the system applied, leaving an incomplete scientific analysis vision. The current study presents a comprehensive analysis of a PV/T system considering the thermodynamic laws to analyse the energy and exergy efficiency of the PV/T system using mono and hybrid nanofluids. A new hybrid nanofluid of titanium oxide-Iron oxide ($TiO_2$–$Fe_2O_3$) with a 50:50 mixing ratio has been synthesised and used as a cooling fluid at different volume fractions was circulated in serpentine tubes soldered on an absorber plate palced at the rear of the PV/T system. Uncertainty analysis and economic analysis are performed to confirm the precision of measured data and evaluate the payback period, the results from prior experiments were used to validate the practicality of the cooling method employed.

## 2. Materials and methods

### 2.1. PV/T system configuration

The PV/T system was built with some modifications to its components to improve its performance compared with a conventional one. A heat exchanger was combined with a polycrystalline PV module (50 W) to improve electrical efficiency by lowering the temperature of the PV cells and absorbing the extra heat from the rear of the module. The excess heat was then converted to thermal energy for use in other applications. The heat exchanger consists of serpentine tubes 5.8 m and copper absorb plates soldered together and placed at the rear of the PV module. The distance between the serpentine tube's arrangement was reduced to 5 cm for increased heat exchange. Thermal grease of high thermal conductivity was used to bond the heat exchanger with the rear of the PV module to ensure perfect contact and avoid heat losses due to air gaps. A new insulation layer type SLENTEX of high insulation was placed on the heat exchanger. Subsequently, an aluminium plate used to cover the heat exchanger to minimise heat dissipation. Another PV module without cooling was used as a comparison to show how the cooling fluid affected the PV module's efficiency and to contrast its performance with the PV/T system. Thermocouples of T type were distributed on the PV/T system's surface, rear, inlet, and outlet and inside the tanks to measure the temperature variation, as shown in Fig. 1.

A helical copper coil was placed into the water tank, which has two ports; one of them is in contact with the outlet of the PV/T system, and the other is connected with a nanofluid tank, helping dissipate the heat and then reducing the nanofluid temperature. The working fluid was circulated by a pump placed inside the nanofluid tank. A flow sensor was fixed between the inlet port and pump to check the mass flow rate. The ambient temperature was detected using a thermocouple, and the solar radiation was measured every 10 min using a solar sensor. Table 1 shows the instruments and device specifications used in the present study. The PV/T system was fixed at a tilt angle of 14.8° towards the south near the University of Miskolc. Fig. 1 illustrates the experimental setup of the PV/T system in conjunction with the reference PV module. The NI cDAQ-9178, a 24-channel data recorder manufactured by National Instruments, was utilized to quantify sun radiation, flow rate, voltages, currents, and temperatures. In Signal Express 2015, the software was linked to



**Fig. 1.** Experimental setup (1) reference PV module, (2) PV/T system, (3) nanofluid tank, (4) water tank, (5) data logger, (6) solar radiation sensor, (7) inlet, (8) outlet, (9) flow sensor, (10–17) thermocouples.

**Table 1**
Specifications sensors and devices measuring.

| Item | Model | Range | Precision | Units |
|---|---|---|---|---|
| Solar sensor | SS11.303 | 1–3999 | ±0.1 | W/m² |
| Thermocouples | T-type 0.2 mm | −250 to 400 | ±0.5 | °C |
| Pump | AD20P-1230C | 240 | – | L/h |
| Flow rate sensor | YF-S201 | 1–30 | ±10% | L/min |
| Voltage sensor | Module 25 V | up to 25 | 0.02445 | V |
| Current sensor | ACS712 | up to 30 | 0.04 | A |
| Electronic scale | BOECO BAS | 3 | 0.0001 g | kg |
| Ultrasonicator | Bransonic | 240:48 | – | Vf/kHz |

the data logger to collect and retrieve data at 10-min intervals.

### 2.2. Synthesis of mono and hybrid nanomaterials

#### 2.2.1. Titanium oxide nanowires (TiO₂ NWs)

$TiO_2$ NWs were produced using a hydrothermal method, as published in our earlier work [21]. The homogenous suspension was formed using 3 g of $TiO_2$ nanoparticles dissolved in 100 mL KOH aqueous solution (10 M) and kept stirred for 30 min, then transferred to a Teflon®-lined autoclave at 160 °C for 24 h. The product was then collected using vacuum filtration and washed several times with 0.1 M HCl and deionised water until the pH value became 7 after drying the products overnight in a furnace. The white $TiO_2$ NWs powder was obtained and calcined at 400 °C for 1 h. As seen in Fig. 2(a), XRD has been used to identify and characterise the crystal structure of $TiO_2$ NWs. The diffraction peaks are located at 33.8°, 39.2°, 48.0°, 54.2°, 56.5°, 66.4° and 68.8°, corresponding to (211), (220), (200), (105), (213), (004) and (403) refer to anatase phase (JCPDS 21-1272). The other peaks located at 27.4°, 36.1° and 41.2° index to (110), (101) and (111) relate to the rutile phase (JCPDS no-21-1276). Furthermore, the diffraction peaks located at 11.4°, 24.1°, 29.2°, 42.9° and 59.8° corresponding to (200), (310), (602) and (610) refer to $K_2Ti_6O_{13}$ (PDF no. 40-0403). All these results agreed with [21,22]. A transmission electron microscopy TEM technique was used for investigations of the surface morphology of $TiO_2$, which is shown as nanowires in Fig. 2(b). The diameter range of nanowires was between 5 and 15 nm with lengths up to 1 μm.

#### 2.2.2. Hybrid titanium oxide/iron oxide (TiO₂ NWs/Fe₂O₃ NPs) nanocomposite

$TiO_2$ NWs/$Fe_2O_3$ nanocomposite has been produced according to our previous work [21]. To make a homogeneous solution, 100 mL of distilled water were used to dissolve the $FeCl_3\cdot6H_2O$ precursor. Then, 0.5 g of $TiO_2$ NWs that had already been produced were added to the solution. Drop by drop, NaOH solution was added while stirring, and when the solution had become base, it was poured into the autoclave and heated to 90 °C for 9 h. The product was dried, calcined at 500 °C for 2 h, and then rinsed with DI water to neutralise pH. The final composition of $TiO_2$NWs- $Fe_2O_3$ is 50:50 w%. To identify and characterise the nanocomposite material's crystal structure, XRD was used. $K_2Ti_6O_{13}$ (PDF no. 40-0403) is the source of the diffraction peaks at 11.9°, 24.2°, 29.1°, 43.1°, and 60°, which correspond to (200), (002), (310), (602), and (610). The anatase phase of $TiO_2$ is related to the other peaks at 39.2°, 48°, 54.2°, 56.5°, and 68.8°, which correspond to (220), (200), (105), (213), and (403). (JCPDS 21-1272). The rutile phase is shown by the diffraction peaks at 27.4°, 36.1°, and 41.2° index to (110), (101), and (111) (JCPDS no-21-1276). The peaks relate to Hematite iron
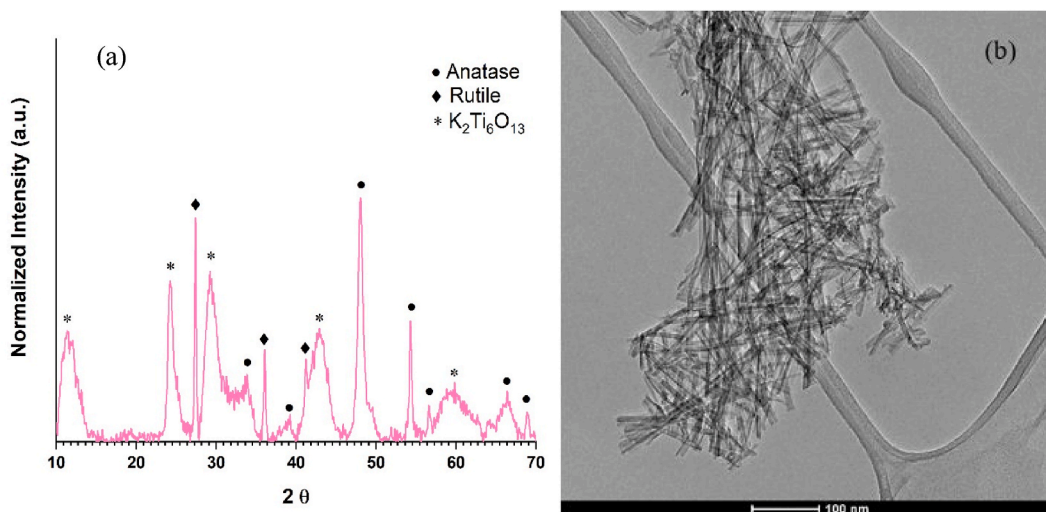


**Fig. 2.** XRD pattern (a) and (b) TEM image of synthesised TiO₂ nanowires.

oxide ($\alpha$-Fe$_2$O$_3$) (JCPDS 33-0664) located at 62.4°, 64° and 67.1°, as shown in Fig. 3(a). These results are in good agreement with [23]. A transmission electron microscopy TEM technique is used to investigate the surface morphology of a hybrid nanocomposite, showing the superposition of TiO$_2$ with Fe$_2$O$_3$, as shown in Fig. 3(b). Fe$_2$O$_3$ nanoparticles dispersed homogeneously on the TiO$_2$ nanowire's surface can be seen in Fig. 3(b).

## 2.3. Preparation of nanofluid

Preparing stable nanofluids is an important feature and achieving that it's not easy. Several matters should be considered to lower the sedimentation of nanomaterials in base fluid and prepare stable nanofluids, such as nanomaterial types, their purity, size, shapes and type of host fluid, and preparation method. The main objective of preparing nanofluids is to enhance the thermal properties of the working fluids, which are used for thermal applications. The two-step method is used to prepare nanofluid, which disperses nano-materials at different volume fractions into base liquids. A certain amount of nanoparticles dispersed in the base fluid aid improve the heat transfer rate and, as a result of the high thermophysical properties of the nanomaterial, the thermal properties of the new working fluid. In this work, the TiO$_2$ nanofluid and hybrid TiO$_2$–Fe$_2$O$_3$ nanofluids have been prepared by the two-step method by dispersion of two volume fractions 0.2% vol and 0.3 vol% of TiO$_2$ NWs and TiO$_2$–Fe$_2$O$_3$ nanocomposite in DI water. First, a specified amount of nanomaterials was distributed in the base fluid, stirred for 30 min with a magnetic stirrer, and scaled using an electronic scale (BOECO BAS of 0.0001 g). For 45 min, a Bransonic 220 ultrasonication probe (Voltage: 240 V, Vf: 48 kHz) was used to prevent nanoparticle agglomeration in the base fluid and to create a stable suspension that would last for a long time. As seen in Fig. 4, visualisation and sedimentation techniques were employed to assess the stability of the nanofluid 4 h after the sonication period and two days later to determine the stationary sedimentation of the nanomaterials in the base fluid. Good stability was shown in both nanofluids prepared. The nanofluids were later prepared in the required quantities and directly used in the experiments after the sonication time.

## 2.4. Thermodynamic analysis

### 2.4.1. Energy evaluation

This section evaluates the PV/T system energy and exergy according to thermodynamics laws. The first law of thermodynamics is to evaluate the PV/T system's performance by determining the energy quantity produced by the PV/T system, including thermal and electrical efficiency. The electrical efficiency is affected by the voltage and current produced by PV cells due to the incident solar radiation. The electrical power produced, solar radiation, and the PV/T system area are the main parameters affecting in electrical efficiency. Eq (1) is applied to determine the electrical efficiency [24]. The other efficiency that results from extracting excess heat from the PV module's back is known as thermal efficiency, and it is influenced by the fluid's characteristics, mass flow rate, and temperature differential while considering solar radiation and system area.

$$\eta_{el} = \frac{P_{out}FF}{A\ S} \tag{1}$$

$$FF = \frac{V_{mp}I_{mp}}{V_{oc}I_{sc}} \tag{2}$$

The average temperature $T_{avg}$ is measured by Eq (3) which represents the average temperature of the surface ($T_{surface}$) and back side
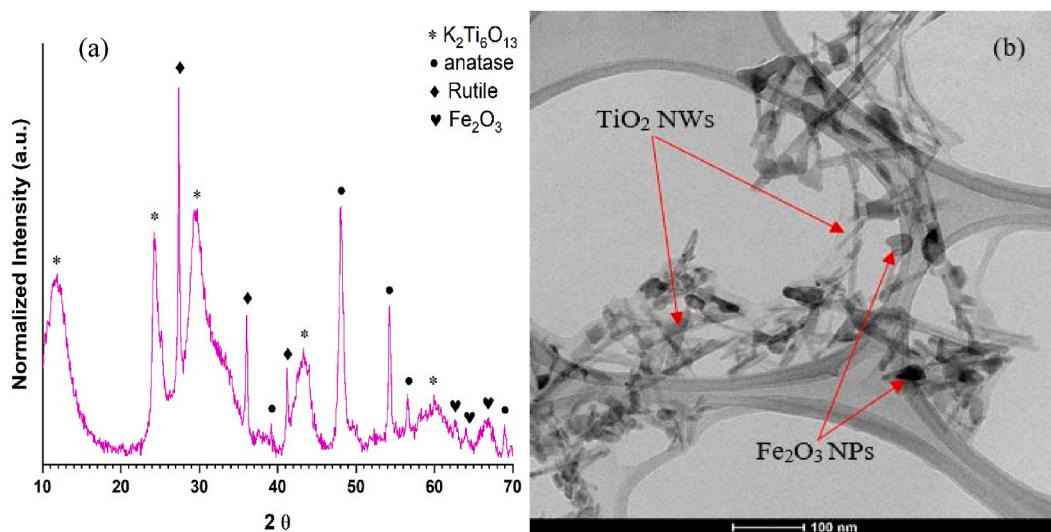


**Fig. 3.** The XRD pattern (a) and (b) TEM image of synthesised TiO$_2$– Fe$_2$O$_3$ nanocomposite.
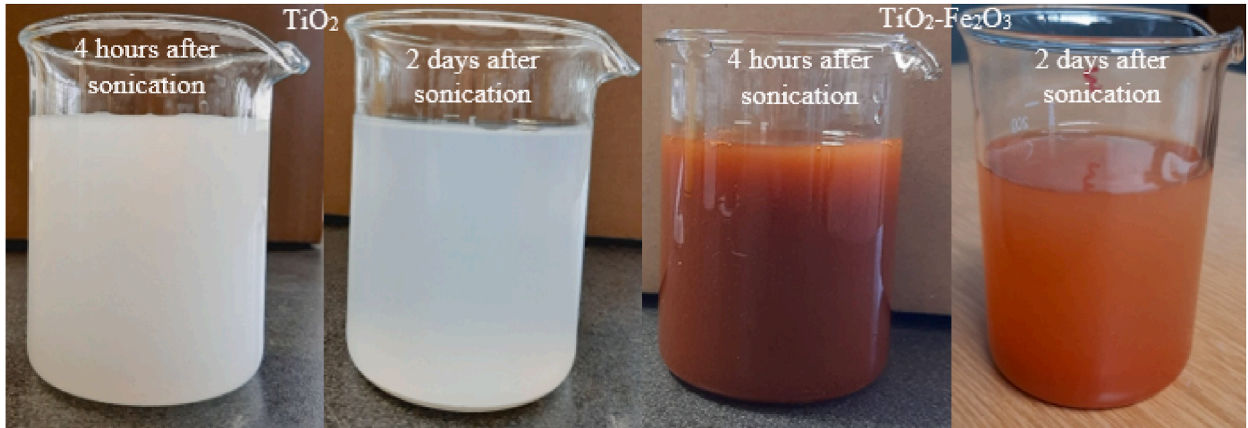
**Fig. 4.** Nanofluid stability during various periods.

($T_{back}$) of the PV/T system, measured by thermocouples.

$$T_{avg} = \frac{T_{surface} + T_{back}}{2} \tag{3}$$

where, $P_{out}$ is the electrical power ($V_{out} \times I_{outF}$), $V_{out}$ is the output voltage, $I_{out}$ is the output current, and FF is the fill factor which represents the maximum electrical power conversion efficiency of the PV module [25] calculated from Eq. (2). S is the solar radiation and A is the PV/T module area. The heat transfer from the rear of the PV module to the absorbing plate and then to the fluids circulating in tubes helps to remove the heat of the PV cells and then increase the thermal efficiency, which determines by Eq. (4) [26].

$$\eta_{th} = \frac{\dot{m}C_p(T_{out} - T_{in})}{A\,S} \tag{4}$$

where $\dot{m}$, is the mass flow rate, $C_p$ specific heat of the fluid, $T_{in}$, and $T_{out}$ inlet and outlet temperatures of the fluid, respectively. The overall efficiency is the sum of thermal and electrical efficiencies calculated from Eq. (5) [27].

$$\eta_{ov} = \eta_{el} + \eta_{th} \tag{5}$$

Thermophysical properties of the circulating fluid affect the heat transfer properties, which influence the PV/T performance. The flow pattern affects the heat removal rate during fluid circulation in tubes placed to the rear of the PV module. Reynolds number has been used to predict flow patterns and calculated by Eq. (6) [28] considering the mass flow rate $\dot{m}$, the viscosity of working fluid $\mu_f$ and hydraulic diameter $D_h$.

$$\mathrm{Re}_{nf} = \frac{4\dot{m}}{\pi \mu_f D_h} \tag{6}$$

*Nu* number is the ratio of heat convection to heat conduction, determined with Eq (7) [29].

$$Nu_{nf} = \left(\frac{hD_h}{K_{nf}}\right) = \frac{\dot{m}C_p(T_{h,i} - T_{h,o})}{A(T_{avg} - T_w)} \times \frac{D_h}{K_{nf}} \tag{7}$$

where h and Tw are the HTC and average wall tube temperature. Because of an increase in viscosity and density brought on by an increase in the volume fraction in the base fluid, the friction factor is a metric that affects the pressure drop in response to changes in Reynold's number. Eq. (8) and (9) are used to calculate both friction factor and pressure drop [30,31].

$$f = [1.58\,ln\ Re - 3.82]^{-2} \tag{8}$$

$$\Delta P = \frac{f\rho_f L}{2D_{tubes}}\left(\frac{4\frac{m_f}{n}}{\rho_f \pi D^2}\right)^2 \tag{9}$$

where L is the riser length and n is the number of tubes.

### 2.4.2. Exergy evaluation

The second law of thermodynamics is utilized to evaluate the exergy quality of the PV/T system, which includes exergy efficiency, losses, and entropy creation [32]. This is necessary to assess the PV/T systems' true performance as well as the electrical and thermal

exergy quality [33]. As seen in Fig. 5, determining the control volume of the PV/T system as well as its input and output that influence the exergy is necessary for evaluating the exergy of the system. Eq. (10) [34] represents the PV/T system's energy balance assuming that it is in a semi-steady state.

$$\sum \dot{E}x_{in} = \sum \dot{E}x_{out} + \sum \dot{E}x_{loss} \tag{10}$$

The inlet exergy $\dot{E}x_{in}$ is the sum of solar exergy ($\dot{E}x_{solar}$) (which represents the incident sunlight absorbed by the PV/T system and could be calculated by Eq. (11)) [35] and the cooling fluid inlet to the system.

$$\dot{E}x_{in} = \dot{E}x_{sun} = S\left(1 - \frac{T_{amb}}{T_{sun}}\right) \tag{11}$$

where $T_{amb}$, is the ambient temperature and $T_{sun}$ is the sun temperature (=5800 K) [36]. The output exergy ($\dot{E}x_{out}$) is the sum of thermal ($\dot{E}x_{ther}$) and electrical energy ($\dot{E}x_{ele}$). Equation (12) is used to compute the thermal exergy [37]. The electrical power energy generated can be computed using Eq. (13), which equals the electrical exergy [38].

$$\dot{E}x_{th} = \dot{m}\,C_{p,f}\left[\left(T_{fout} - T_{fin}\right) - T_{amb}\,\ln\left(\frac{T_{fout}}{T_f in}\right)\right] \tag{12}$$

$$\dot{E}x_{ele} = P_{pv}\,\text{FF} \tag{13}$$

Equations (14) and (15) can be used to determine the thermal and electrical exergy efficiencies of the PV/T system [34].

$$\eta_{\dot{E}x_{ther}} = \frac{\dot{m}C_{p,nf}\left[\left(T_{f,out} - T_{f,in}\right) - T_{amb}\,\ln\left(\frac{T_{f\,out}}{T_{fin}}\right)\right]}{S\left(1 - \frac{T_{amb}}{T_{sun}}\right)} \times 100 \tag{14}$$

$$\eta_{\dot{E}x_{ele}} = \frac{P_{pv}\text{FF}}{S\left(1 - \frac{T_{amb}}{T_{sun}}\right)} \times 100 \tag{15}$$

The exergy efficiency is the sum of thermal and electrical efficiencies of the PV/T system, which is calculated by Eq. (16).

$$\eta_{\dot{E}x} = \frac{\dot{E}x_{ther} + \dot{E}x_{ele}}{\dot{E}x_{solar}} \times 100 \tag{16}$$

Because of the frictional and heat transfer losses in the system, energy destruction, or energy losses, is a significant parameter. Entropy generation $\dot{S}_{gen}$ or irreversibility is a thermodynamic parameter that indicates that irreversibility occurs in the system [39]. Both parameters can be calculated by Eqs. (17) and (18) as follows:

$$\dot{E}x_{losses} = \dot{E}x_{in} - \dot{E}x_{ele} - \dot{E}x_{ther} \tag{17}$$

$$\dot{S}_{gen} = \frac{\dot{E}x_{lost}}{T_{amb}} \tag{18}$$

### 2.4.3. Thermophysical properties of nanofluids

Solid materials are characterised by higher thermal properties than liquids. The dispersion of a specific amount of nanomaterials in the base fluid results in the creation of a novel fluid with enhanced thermal characteristics compared to the base fluids. Thermal conductivity, specific heat, density, and viscosity are the most effective properties significantly affecting nanofluid performance. In the present study, the nanomaterials were synthesised, and then their thermophysical properties were measured, particularly hybrid $TiO_2$–$Fe_2O_3$ nanocomposite, while those of the mono $TiO_2$ NWs were adopted from previous studies. The thermophysical properties of the hybrid $TiO_2$–$Fe_2O_3$ nanocomposite have been measured at the polymer department of the University of Miskolc. The thermal
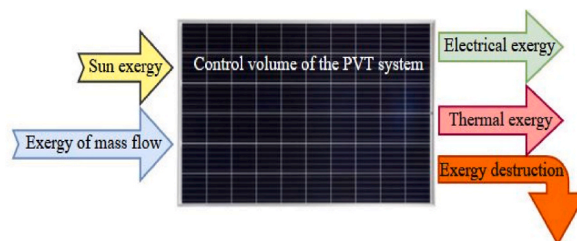
**Fig. 5.** The exergy flow of a PV/T system.

conductivity of $TiO_2$–$Fe_2O_3$ nanocomposite was measured by a thermal conductivity analyser (C-Therm TCi), and the specific heat of the nanocomposite was measured by Mettler-Toledo DSC 823e. On the other hand, the density and viscosity of nanocomposite were measured using pycnometer A and IKA Rotavisc lo-vi rotational viscosimeter. The nanofluid density is an essential property affecting nanofluid stability and the system's thermal sustainability. Eq. (19) is used to calculate the density of nanofluid [40]. The heat transfer field is greatly impacted by a nanofluid's thermal conductivity, and enhancing this attribute can improve the nanofluid's thermal performance, which can be computed using Eq. (20) [41]. The specific heat plays a vital function in transferring energy between bodies. The specific heat of a nanofluid is contingent upon the type of base fluid, the nanomaterials employed, and their concentration within the base fluid Eq. (21) is used to calculate the specific heat of the nanofluid [42]. Viscosity is not less important than density, which has essential effects on the nanofluids' behaviour and pumping power of the thermal system. Eq. (22) is used to calculate the viscosity of nanofluids [43]. Table 2 shows the thermophysical properties of mono and hybrid nanocomposites.

$$\rho_{nf} = \varphi \cdot \rho_{np} + (1 - \varphi) \cdot \rho_{bf} \tag{19}$$

$$\frac{k_{nf}}{k_{bf}} = \frac{k_{np} + 2k_{bf} + 2\varnothing\left(k_{np} - k_{bf}\right)}{k_{np} + 2k_{bf} - \varnothing\left(k_{np} - k_{bf}\right)} \tag{20}$$

$$C_{p,nf} = \frac{\varphi \cdot \left(\rho_{np} \cdot C_{p,n}\right) + (1 - \varphi) \cdot \left(\rho_{bf} C_{p,bf}\right)}{\rho_{nf}} \tag{21}$$

$$\mu_{nf} = \frac{\mu_{bf}}{(1 - \varnothing)^{2.5}} \tag{22}$$

$$\varphi = \left[ \frac{\frac{m_{ap}}{\rho_{np}}}{\frac{m_{np}}{\rho_{np}} + \frac{m_{bf}}{\rho_{bf}}} \right] \times 100 \tag{23}$$

where $k_{np}, k_{nf}$ and $k_{bf}$, are the thermal conductivity of nanomaterials, nanofluid and base fluid. $\varphi$ is the volume fraction of nano-materials dispersion in the base fluid, which was calculated from Eq. (23), $m_{bf}$ $m_{np}$ are the mass of the base fluid and nanomaterials. $C_{p,nf}, C_{p,np}$ and $C_{p,bf}$ are the specific heat of the nanofluid, nanomaterials and base fluid and respectively. While $\rho_{np}$ $\rho_{nf}$ and $\rho_{bf}$ are the density of nanomaterials, nanofluid, and base fluid, respectively.

### 2.5. Uncertainty analysis

To perform a valid test, it is necessary to evaluate errors that may occur due to human measurements during experiment mea-surements or calibration. Ensuring the accuracy of the collected data is crucial for establishing the reliability of the acquired results. Uncertainty analysis applied by J. Michael and S. Iniyan [46] is adopted in this study with negligible PV/T system size and the specific heat of the working fluid. The uncertainty measurements of thermal and electrical efficiencies could be determined according to Eqs. (24) and (25) as follows:

$$\eta_{therm} = f(T, \dot{m}, S) \tag{24}$$

$$\eta_{elec} = f(I, V, S) \tag{25}$$

where $\dot{m}$, I, T, S and V are the accuracies of water mass flow rate, current, temperature, solar radiation, and voltage sensors and devices used (Table 1). The uncertainty in thermal and electrical efficiencies was 1.47% and 1.08%, respectively. Thereby, the uncertainty equations are expressed in Eqs. (26) and (27), where U is the uncertainty.

$$\left[\left(\frac{U_{\eta_{therm}}}{U_{\eta_{therm}}}\right)^2\right]_{therm} = \sqrt{\left(\frac{U_{\dot{m}}}{\dot{m}}\right) + \left(\frac{U_S}{S}\right) + \left(\frac{U_T}{T}\right)} \tag{26}$$

$$\left[\left(\frac{U_{\eta_{elec}}}{\eta_{elec}}\right)^2\right]_{elec} = \sqrt{\left(\frac{U_v}{V}\right) + \left(\frac{U_I}{I}\right) + \left(\frac{U_S}{S}\right)} \tag{27}$$

**Table 2**
Characteristics of the nanomaterials and DI water.

| Properties | $TiO_2$–$Fe_2O_3$ | $TiO_2$ [44,45] |
|---|---|---|
| Density (kg/m³) | 3473 | 3900 |
| Thermal conductivity (W/m·K) | 75.32 | 8.9 |
| Heat capacity (J/kg·K) | 1321 | 686 |
| Viscosity (kg/ms) | 0.00503 | 0.00213 |

*2.6. An economic evaluation of the PV/T system*

An essential aspect is to conduct an economic study of the suggested cooling method in contrast to the traditional PV module. This analysis is crucial in determining the payback period [47] and assessing the viability of a long-term hybrid PV/T system. The economic analysis could be achieved considering the daily maintenance (may be non-existent on some days of the month), operation cost (including pump and flow sensor), electrical consumption and others. The cost of nanofluid has significantly dropped through the laboratory synthesis of nanomaterials and subsequent creation of the nanofluid. This approach also offers the potential for enhanced purity and morphology of the nanomaterials. The daily cost of the nanofluid was determined by dividing the overall price by the number of days in a year. The PV/T system consists of several components such as an absorber, copper tubes, an aluminium cover, insulation, a pump, a flow sensor, plastic tanks, and so on. The net profit is derived from Eq. (28) [48] considering the cost of each element mentioned in Table 3. Compared with conventional PV modules, the hybrid PV/T system with hybrid nanofluid achieved less payback period of 630 days using $TiO_2$, which has a payback period of 684 days, and conventional PV modules reached about 790 days. This difference makes sense theoretically and confirms that using nanofluids to increase the PV/T system's efficiency and economic feasibility is effective.

$$\text{Net profit} = \text{Cost of energy production (electric and thermal energy)} - \text{Cost of nanofluid} - \text{Cost of operation} - \text{Cost of maintenance} \qquad (28)$$

## 3. Results and discussions

This section covers the energy and energy results of the PV/T system cooled by mono, hybrid, and DI water at different volume fractions. Then the effect of increased volume fraction on improved heat transfer parameters has an impact by decreased PV cells temperature and enhanced energy and exergy efficiency of the PV/T system. The energy and exergy performance of nanofluids in upgrading the PV/T system has been compared with existing literature findings to demonstrate its usefulness. The payback period is assessed to ascertain the viability of employing mono and hybrid nanofluids as cooling agents in PV/T systems.

*3.1. Energy results*

*3.1.1. Temperature profile*

The experiments were conducted in August 2022 at the University of Miskolc, Hungary. The performance of the PV/T system has been enhanced by using a mono $TiO_2$ nanofluid, a hybrid $TiO_2$–$Fe_2O_3$ nanofluid, and DI water as cooling fluids. The results have been compared with a reference PV module. The performance of the PV/T system is influenced by the rise in temperature and the incident solar radiation during the day. Fig. 6(a) shows the average solar radiation values and ambient temperature recorded during the experiment days. The highest solar radiation measured was 918.93 W/m² at 12:20 p.m., and the ambient temperature was 34.16 °C. Thus, increased solar radiation coincides with rising ambient temperature, which affects the PV cells by reducing their conversion efficiency. Fig. 6(b) shows the temperature of the PV module and PV/T system from the beginning until the end of the experiment. The maximum temperature of the reference PV module recorded was 52.61 °C at noon when the maximum ambient temperature of 34.16 °C increased the PV cell's temperature and caused decreased electrical efficiency. The heat exchanger placed at the rear of the PV module helps decrease the PV cell's temperature by circulating fluids in tubes, reducing the absorb plate temperature due to heat transfer convection from the tubes to the circulating fluid. The PV cell's temperature is reduced due to the heat transfer from the rear of the PV module to the absorbing plate by conduction. The temperature of the PV cells in the PV/T system has been decreased to 50.65 °C by circulating DI water. This decrease is a result of removing heat from the rear of the PV module, which has caused a reduction in the temperature of the PV module by around 3.87%. Circulation of $TiO_2$ nanofluid at varying volume fractions (0.2 vol% and 0.3 vol%) resulted in a decrease in the PV temperature to 47.31 °C and 46.11 °C, respectively. Reduced temperature is attributed to the high thermal properties of $TiO_2$ NWs dispersed in the DI water, which improved the fluid thermal properties, such as thermal conductivity. Thus, reducing the PV module temperature by 14% at 0.3 vol% compared with the reference PV module and 9.84% compared with the cooling by DI water. Fig. 6(b) illustrates the impact of employing a hybrid nanofluid as a cooling medium in decreasing the temperature of the PV module compared to cooling with DI water and mono nanofluid. The addition of $Fe_2O_3$ nanoparticles onto the $TiO_2$ nanowires has enhanced the surface area of the nanocomposite when it is suspended in the base fluid. This improvement has resulted in

**Table 3**
PV module and PV/T system economic analysis using hybrid nanofluid cooling.

| Elements/aspects | PV/T system | PV/T system | Conventional PV |
|---|---|---|---|
| Configuration | 179.86 $ | 179.86 $ | 39.76 $ |
| Maintenance | 0.007 $/day | 0.007 $/day | 0.00397 $/day |
| Nanofluid supply | 0.06 $/day hybrid nanofluid | 0.0286 $/day mono nanofluid | – |
| Operation cost | 0.00363 $/day | 0.00363 $/day | – |
| Energy productivity | 0.356 $/day | 0.302 $/day | 0.0543 $/day |
| Net profit | 0.285 | 0.2627 | 0.05033 |
| Payback period | 630 days | 684 | 790 days |
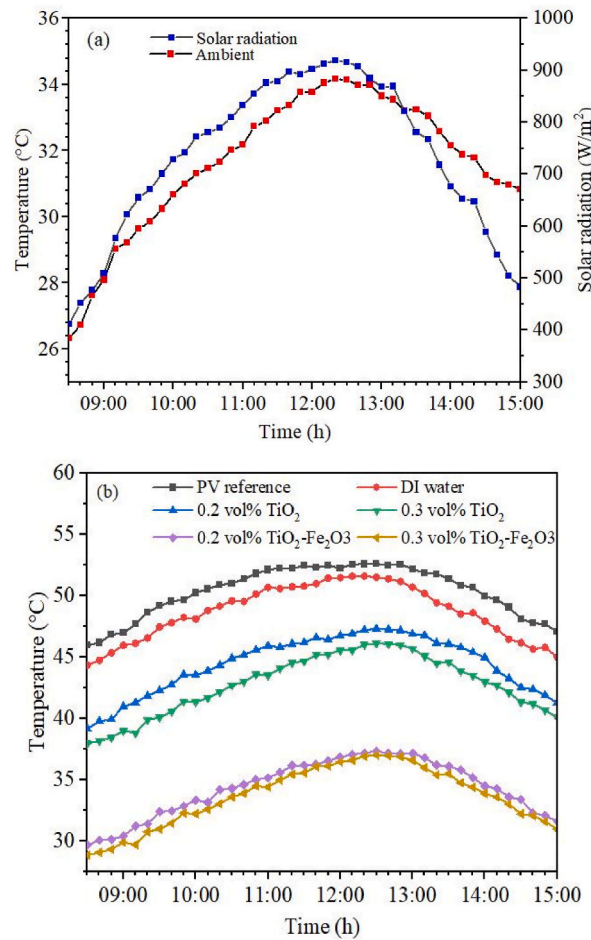
**Fig. 6.** (a) In-site solar radiation and ambient temperature, (b) temperature variation of PV and PV/T system.

enhanced thermal properties, leading to an increase in convective heat transfer and a decrease in the temperature of the PV module. The flow of a mixture of $TiO_2$–$Fe_2O_3$ nanoparticles and fluid with volume fractions of 0.2% and 0.3% via the serpentine tubes, enhanced the convective heat transfer and effectively removed surplus heat from the PV module, resulting in a temperature reduction of 37.31 °C and 37 °C. The utilization of a hybrid nanofluid at concentrations of 0.2 vol% and 0.3 vol% resulted in a reduction of the temperature of the PV module by 41.11% and 42.19%, respectively, compared to the reference PV module. The resultss of this work demonstrate that hybrid $TiO_2$–$Fe_2O_3$ nanofluids exhibit a higher heat dissipation capability in comparison to mono $TiO_2$ nanofluids when employed as a coolant.

*3.1.2. Performance of PV/T system*

The reference PV module's electrical output was lowered as a result of the PV cell conversion efficiency being impacted by a dip in open-circuit voltage [49], brought on by rising PV cell temperature. The reference PV module recorded a maximum electrical output of 21.61 W. Cooling the PV/T system with DI water resulted in a 3.78% temperature drop and an increase in electrical power to 24.41 W. Increased open-circuit voltage brought about by the cooling fluid's improved thermal characteristics has favorably increased electrical power. In the end, lower PV cell temperatures contributed to a rise in the electrical power output of the PV/T system. Fig. 7(a) illustrates the impact of $TiO_2$ nanofluid at concentrations of 0.2 vol% and 0.3 vol% on enhancing electrical power. The highest electrical power measured was 30.31 W and 31.6 W, respectively. In addition, the electrical power was enhanced by 24.44% and 29.45% compared with the cooling by DI water. This is attributed to enhanced heat exchange between the hot body (backside of the PV module) and the less hot body (absorbing plate), enhancing the PV/T system performance.

On the other hand, the dispersion of $TiO_2$–$Fe_2O_3$ nanoparticles in the DI water significantly enhanced the working fluids' thermal characteristics, boosting the PV/T system's output of electrical power. With the introduction of hybrid $TiO_2$–$Fe_2O_3$, the electrical power was progressively increased to 39 W and 39.71 W, respectively, at varying volume fractions of 0.2 vol% and 0.3 vol%. By increasing the HTC of the nanofluid, which dissipated more heat from the PV cells, the hybrid nanofluid increased the electrical power by 59.775% and 62.67% as compared to the PV/T system cooled by DI water. The overall efficiency of the PV/T system and reference module with cooling by mono and hybrid nanofluid, as well as DI water, is displayed in Fig. 7(b). The electrical efficiency of the PV
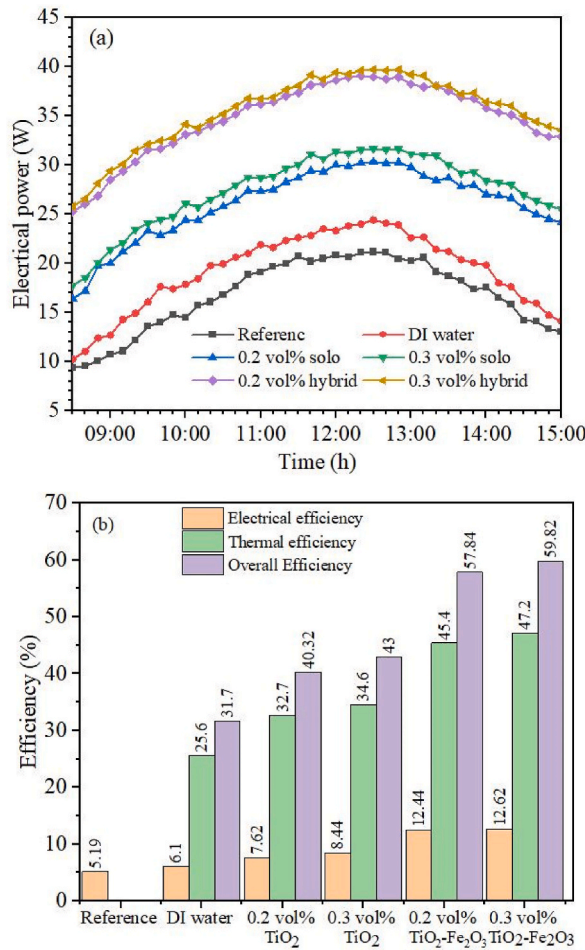
**Fig. 7.** PV and PV/T system performance (a) electrical power, (b) overall efficiency.

module under reference conditions, with maximum solar radiation and room temperature, was 5.19%. The enhanced electrical output of the PV/T system due to cooling directly influences its electrical efficiency. Because DI water is used to cool the PV modules, a modest drop in temperature contributed to a gain in electrical efficiency of 17.53%.

In contrast, the electrical efficiency of the PV/T system was greater when the volume fraction of mono and hybrid nanocomposite in the base fluid was higher, as compared to DI water. $TiO_2$ nanofluid circulation into tubes has increased the heat removal by convection and increased the thermal efficiency to 21.91% and 38.36% at 0.2 vol% and 0.3 vol%, respectively, compared with the DI water. Using hybrid $TiO_2$–$Fe_2O_3$ nanofluid at 0.2 vol%, 0.3 incremented the electrical efficiency by 103.93% and 106.88%, when compared by cooling with DI water due to the improved thermal properties of the hybrid nanofluids. This increment resulted from the increased

**Table 4**
Comparison between the results of the current study and the findings from existing literature.

| Ref. | PV peak power | Nanofluid used | Volume fraction % | Temperature dcreased % | Electrical efficiency % | Thermal efficiency % |
|------|--------------|----------------|-------------------|------------------------|-------------------------|----------------------|
| Current study | 50 W | $TiO_2$–$Fe_2O_3$ | 0.2 | 15.3 | 12.44 | 45.4 |
| | | $TiO_2$–$Fe_2O_3$ | 0.3 | 15.6 | 12.62 | 48.2 |
| [13] | 35 W | $Al_2O_3$/$SiO_2$ | 0.5 | 16.52 | 1.99 | 9.09 |
| [50] | 50 W | $TiO_2$ | 0.3 | 8.2 | 18.8 | 45 |
| [28] | 80 W | $TiO_2$ | 1 | 10.43 | 7.32 | 41 |
| [51] | 250 W | $Al_2O_3$/ZnO–$Fe_3O_4$ | 1 | 3.74 | 13.43 | 54.11 |
| [52] | 250 W | $Al_2O_3$/ZnO | 1.7 | 17.72 | 13.8 | 55.9 |
| [53] | 150 W | CNT/$Al_2O_3$ | 2 | 12.21 | 17.2 | 27.23 |
| [54] | 200 W | $Fe_3O_4$ | 0–1 | – | 12.29–12.38 | 50.89–69.37 |
| [55] | 295 W | MWCNT/$Fe_3O_4$ | 0.048 | 8.9 | 14.56 | 55.42 |
| [56] | 100 W | MWCNT | 0.5 | 17 | 13.2 | 63 |
| [57] | 50 W | $TiO_2$–CuO | 0.2 | 13.7 | 9.2 | 50.2 |
| | | | 0.3 | 14.5 | 10.3 | 41.7 |

surface area of the hybrid nanocomposite dispersed into DI water which increased the thermal conductivity of nanofluids. Heat removal of the rear of the PV module is increased by using a hybrid nanofluid higher than $TiO_2$ nanofluid and DI water, which was observed by temperature drops and improved electrical efficiency. Increased heat removal has incremented the thermal efficiency of the PV system, in which using hybrid $TiO_2$–$Fe_2O_3$ nanofluid had achieved higher thermal efficiency than $TiO_2$ nanofluid by 36.41% at 0.2 vol% and 38.83% at 0.3 vol%.

In contrast, using $TiO_2$ nanofluid had increased thermal efficiency by 27.77% and 35.15% at the same volume fraction. Since the overall efficiency is the sum of thermal and electrical efficiencies, the maximum increment of overall efficiency has been recorded by using a hybrid nanofluid was 88.7% and 39.11% compared with $TiO_2$ nanofluid at 0.3 vol% and cooling by water, respectively. This is attributed to the high thermal properties of the hybrid $TiO_2$–$Fe_2O_3$ nanofluid. As indicated in Table 4, the results obtained are compared with prior research to demonstrate the potential of $TiO_2$–$Fe_2O_3$ nanofluids as a cooling fluid to enhance the performance of PV/T systems. A number of factors were taken into account in the comparison, including the size of the PV/T system, the nanofluids that were employed, the volume percentages of nanocomposite in the base fluid, the measurement conditions and how they affected the temperature drop, and the thermal and electrical energy efficiency of the system.

The current findings may not be superior to those found in previous research, but they do emphasise the significance of the novel kind of nanofluid that may be employed as a cooling fluid to raise the PV/T system's energy and efficiency. The hybrid $TiO_2$–$Fe_2O_3$ nanocomposite's volume fractions that were used improved PV/T performance when compared to DI water and outperformed other studies that used various nanofluids, indicating that the applied nanofluid was effective.

Dispersion of nanomaterials in the host fluid causes an improvement in their thermal properties since nanomaterials have higher thermal properties than conventional fluids. This study investigated the influence of adding $TiO_2$ NWs and $TiO_2$–$Fe_2O_3$ nano-composites at different volume fractions in DI water on Reynolds number, *Nu* number, heat transfer coefficient, pressure drop and friction factor. The heat transfer coefficient, *Nu* number, pressure drop, and fraction factor were calculated considering the maximum, average and minimum (something missed here), according to Eqs. (15)–(17). Fig. 8(a) illustrates how the *Nu* number changes with increasing volume fractions of TiO2 NWs and $TiO_2$–$Fe_2O_3$ nanocomposite, as a function of Reynold's number. It demonstrates a progressive increase in the *Nu* number as Reynold's number increases. The addition of 0.2 vol% and 0.3 vol% of $TiO_2$ NWs to DI water resulted in a 42.68% and 49.72% increase in the maximum value of the *Nu* number of the working fluid, respectively, compared to DI water alone.

When $TiO_2$–$Fe_2O_3$ nanocomposite was suspended in the base fluid at 0.2 and 0.3 vol%, the maximum value of *Nu* number rose by 37–86% and 42.72% compared to $TiO_2$ nanofluid. Because the hybrid nanofluid has better thermal characteristics than $TiO_2$ nanofluid, an increase in *Nu* numbers of the $TiO_2$–$Fe_2O_3$ nanofluid has increased the HTC, which has favorably increased the PV/T system performance. The enhanced HTC with Reynold's number increment at various volume fractions is depicted in Fig. 8(b), and it is explained by the nanofluid's greater thermal conductivity in comparison to DI water. The HTC has increased by 19.6% and 23% over $TiO_2$ nanofluid at used hybrid nanofluid, whereas the HTC has increased by 62.5% and 70.6% over pristine DI water after adding 0.2 vol% and 0.3 vol% of $TiO_2$ NWs to the DI water. When hybrid nanofluid was used instead of mono nanofluid, the HTC was higher due to the enhanced heat exchange between the absorbing plate and the rear of the PV/T system, lowering the PV temperature more than DI water. Because of the strong thermal characteristics, the hybrid nanofluid's density increases along with its volume portion, which affects the pressure drop. A significant problem that affects the fluid flowing through tubes and increases power consumption is the increased density of nanofluid. As a function of the increased Reynolds number used, $TiO_2$ nanofluid with 0.2 vol%, 0.3 vol% has increased the density and viscosity of nanofluid, increasing the pressure drop by 66.2% and 83.16% compared to the DI water. The pressure drops when using $TiO_2$–$Fe_2O_3$ nanocomposite was increased by 35.2% and 45.43% higher than $TiO_2$ nanofluid, which is logical due to the high density of the hybrid nanocomposite compared to $TiO_2$.

Fig. 9(a) shows the pressure drop difference when using mono and hybrid nanofluid. It can be noticed that increased volume
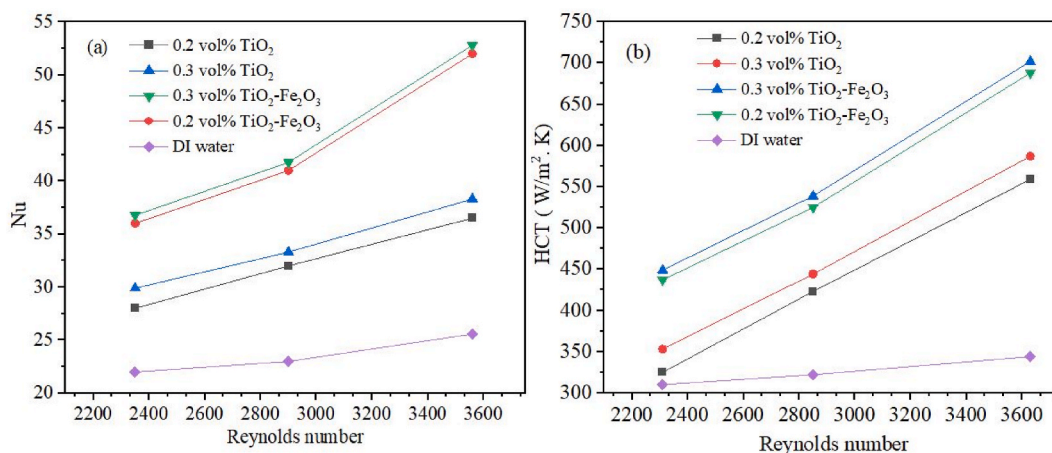


**Fig. 8.** Impact of Reynolds number and volume fractions on (a) *Nu* Number, (b) HTC.

fraction of $TiO_2$–$Fe_2O_3$ nanocomposite at 0.3 vol% resulted a slight increase in the pressure drop. The nanomaterials dispersed in DI water resisted the fluid flow and increased the pressure drop. Therefore, increasing the volume fraction increased the pressure drop. Fig. 9(b) illustrates the reduction in friction factor of the $TiO_2$–$Fe_2O_3$ nanofluid as the Reynolds number and volume percent of the nanocomposite rise in the DI water. The friction factor of DI water was lower than that of nanofluids due to the increased density and viscosity of the hybrid nanofluids. The friction factor decreased by 6.97% and 13.95% when the Reynolds number and volume fraction of $TiO_2$ NWs increased by 0.2 vol% and 0.3 vol%, respectively, compared to DI water. When comparing the use of $TiO_2$ nanofluid with $TiO_2$–$Fe_2O_3$ nanofluid, it was found that the latter resulted in an increase in the friction factor by 18.36% and 23.91% at volume fractions of 0.2 vol% and 0.3 vol%, respectively.

### 3.2. Exergy results

The thermal exergy of the system is proportional to the specific heat of the cooling fluid, the flow rate, and the exit temperature of the cooling fluid. Fig. 10(a) illustrates the thermal exergy of the PV/T system using $TiO_2$ and $TiO_2$–$Fe_2O_3$ nanofluids in comparison to DI water. It is observed that increasing nanomaterials concentration in the base fluid had incremented the thermal exergy of the system. Dispersion of 0.3 vol% and 0.2 vol% of $TiO_2$–$Fe_2O_3$ nanocomposite in the DI water had increased the thermal exergy by 38.37% and 46.37% higher than the $TiO_2$ nanofluid. This is attributed to improved nanocomposite thermal conductivity, which enhanced the convective heat transfer between circulating cooling fluid and tubes placed on the absorbing plate. On the other side, increasing volume fractions of $TiO_2$ NWs in the DI water achieved a 16.64% and 27.18% increment of thermal exergy compared to the pristine DI water. However, it is evident that thermal exergy has a lesser value compared to the electrical exergy. This is because the outlet temperatures of the circulated fluid converge with the ambient temperature, as demonstrated by Chow [58]. The maximum thermal and electrical exergies were recorded at the solar noon, which is attributed to solar radiation perpendicular to the PV module surface. Thus, enhancing thermal properties, such as the thermal conductivity and specific heat of the cooling fluid, may achieve comparable results with electrical exergy.

The output fluid temperature has an impact on the thermal exergy efficiency of the system, as indicated by Equation (14). Fig. 10(b) demonstrates that when the concentration of $TiO_2$ nanoparticles in DI water increases, there is a steady improvement in the thermal exergy efficiency. At a concentration of 0.2 vol%, the efficiency reaches around 25.43%, and at 0.3 vol%, it reaches about 39.8%. These values are in comparison to the thermal exergy efficiency of DI water alone. The thermal efficiency of hybrid nanofluids has been increased by 49.4% and 63.81% more than that of $TiO_2$ nanofluids with the same volume fractions. It can be observed that the thermal exergy efficiency was much lower than the electrical exergy efficiency. This is attributed to the low quality of the thermal exergy, one of the reasons that reduced the thermal exergy efficiency, which agrees with the findings of Sardarabadi et al. [24]. The electrical exergy efficiency was relatively enhanced with the increased volume fractions. The maximum electrical exergy recorded was 12.27% and 12.49% when using $TiO_2$–$Fe_2O_3$ nanocomposite at 0.3 vol% and 0.2 vol%.

Conversely, the use of $TiO_2$ nanofluid for cooling resulted in a smaller increase in electrical exergy efficiency, specifically by approximately 7.49% and 8.36%, as compared to the use of hybrid nanofluid at volume fractions of 0.3 vol% and 0.2 vol%, as depicted in Fig. 10(b). Thus, using $TiO_2$–$Fe_2O_3$ nanofluid has increased the electrical exergy efficiency of the PV/T system higher than $TiO_2$ nanofluid by 49.4and 63.81% due to increased surface area of the hybrid nanomaterials and its higher thermal properties which positively reduced the temperature of PV cells and enhanced their overall exergy efficiency. An increment in the electrical energy efficiency has significantly increased the overall exergy of the PV/T system than the thermal exergy efficiency. It can be observed that increasing the volume fraction of $TiO_2$–$Fe_2O_3$ nanocomposite in the base fluid has increased the overall exergy to about 53.82% and 67% at 0.2 vol% and 0.3 vol%, respectively, compared with the $TiO_2$ nanofluid. Table 5 presents the impact of mono $TiO_2$ and hybrid $TiO_2$–$Fe_2O_3$ nanofluids on the thermal and electrical exergy efficiencies of the PV/T system in this work, in comparison to previous
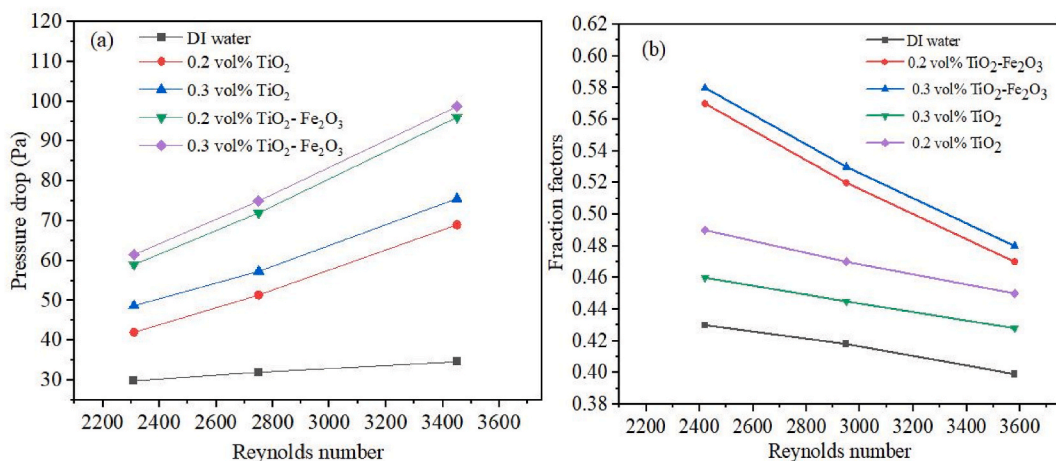
**Fig. 9.** Impact of Reynolds number and volume fraction on (a) pressure drop, and (b) friction factor.
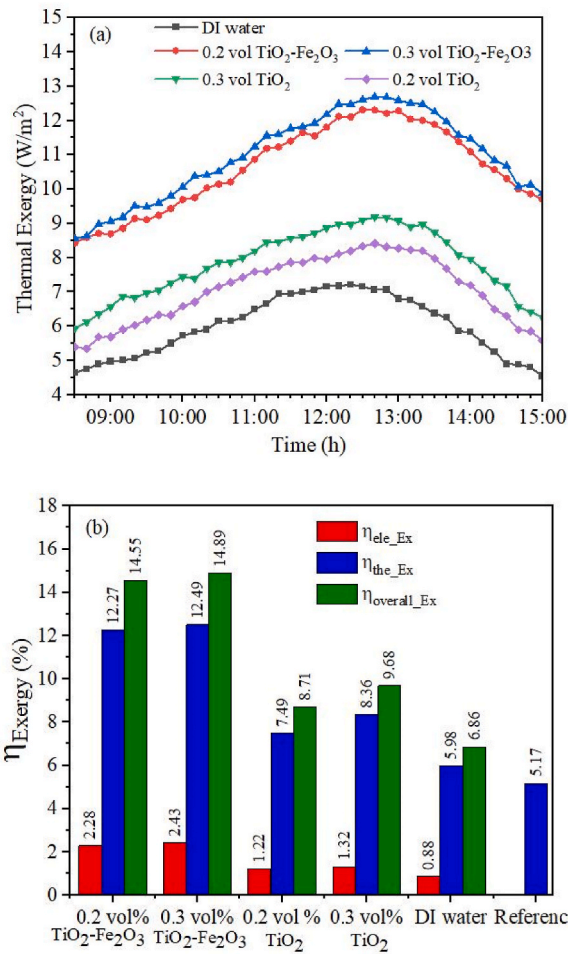
**Fig. 10.** Exergy performance of the PV and PV/T system (a) thermal exergy, (b) overall exergies.

studies that used different PV/T system sizes, volume fractions, and types of nanomaterials. The exergy study results demonstrated that the hybrid TiO₂–Fe₂O₃ nanofluid had a greater influence on both thermal and electrical exergy efficiency compared to TiO₂ nanofluid and other nanofluids. Nevertheless, the restricted dispersion of TiO₂–Fe₂O₃ nanocomposite in the underlying fluid yields superior exergy efficiency in comparison to previous research, thereby confirming the efficacy of hybrid nanofluids for cooling purposes.

Evaluating energy dissipation and entropy production in thermodynamic systems is crucial for quantifying system losses and

**Table 5**
A comparison between the current study exergy performance and other studies.

| Ref. | PV peak power | Type of nanofluid | volume fraction% | Thermal exergy % | Electrical exergy % |
|---|---|---|---|---|---|
| Current study | 50 W | TiO₂–Fe₂O₃ | 0.2 | 2.28 | 12.27 |
| | | | 0.3 | 2.43 | 12.49 |
| | | TiO₂ | 0.2 | 1.22 | 7.49 |
| | | | 0.3 | 1.32 | 8.36 |
| [59] | 50 W | WO₃ | 0.5 | 0.76 | 7.87 |
| | | | 0.75 | 0.91 | 8.81 |
| | | | 1 | 1.2 | 9.3 |
| [60] | 40 W | Al₂0₃ | 0.2 | 1.01 | 10.87 |
| | | ZnO | 0.2 | 1.18 | 10.99 |
| | | TiO₂ | 0.2 | 0.91 | 11.02 |
| [32] | 60 W | Carbon black | 0.1 | 0.25 | 15.25 |
| | | | 0.2 | 0.52 | 15.98 |
| | | | 0.3 | 0.34 | 15.55 |
| | | | 0.4 | 0.19 | 14.45 |
| [24] | 40 W | ZnO | 0.2 | 0.89 | 11.48 |
| | | PCM | – | 1.6 | 12.01 |

irreversibilities. Equations (17) and (18) are used to calculate the exergy loss and entropy generation of the PV/T system using DI water, mono, and hybrid nanofluids at different volume fractions. Increased energy losses occur when the PV module's temperature is raised. Employing a hybrid nanofluid has improved thermal properties and reduced the exergy losses. Fig. 11 shows the relatively reduced exergy losses of the PV/T system compared with the reference PV module. Cooling the PV/T system with water has decreased the exergy losses by 7.31% compared with the reference PV module. Exergy losses have decreased by 15% and 19.11% with the cooling by $TiO_2$ nanofluid at 0.2 vol% and 0.3 vol%. Circulation of hybrid $TiO_2$–$Fe_2O_3$ nanofluid in tubes has reduced the exergy losses of the PV/T system by 40.58% and 45.5% more than the $TiO_2$ nanofluid due to the increased conversion rate of the heat generated from the PV cells to useful thermal energy. Conversely, the PV temperature increase and enhanced heat transmission between the PV/T system and the surroundings led to the greatest amount of entropy generation in the standard PV module. Increasing volume fractions have enhanced the electrical exergy efficiency due to the reduced temperature of PV cells, and reduced entropy generation. Fig. 11 shows the effect of cooling by DI water and nanofluids. The use of DI water as a cooling agent in the PV/T system has resulted in a 12% decrease in entropy generation compared to the reference module. However, when the system is cooled using $TiO_2$ nanofluid at a concentration of 0.3 vol%, the entropy generation increases to 26.38%. The use of a $TiO_2$–$Fe_2O_3$ nanofluid at a concentration of 0.3% in the PV/T system has resulted in a reduction of entropy generation by 86.29% compared to the use of a $TiO_2$ nanofluid. In comparison to the mono nanofluid and DI water, the hybrid nanofluid led to reduced exergy losses and entropy creation in the PV/T system during cooling. Reducing the quantity of work lost in the PV/T system is essential.

## 4. Conclusions

This work conducted an experimental investigation to examine the impact of mono and hybrid nanofluids on the energy and exergy performance of the PV/T system at various volume fractions. Additionally, a cost-benefit analysis is performed to show that the cooling mechanism used is viable. The primary results are succinctly summarised in the sections that follow:

- The hybrid $TiO_2$–$Fe_2O_3$ nanocomposite and mono $TiO_2$ NWs have been successfully synthesised using a hydrothermal method which led to improving the thermal conductivity of the nanocomposite to 75.32 W/m·K and specific heat to 1321 J/kg K by compared when used separately.
- The reference PV module recorded a maximum temperature of 52.61 °C reduced by 3.87%, 14% and 42.18% when cooling by DI water, mono and hybrid nanofluids at 0.3 vol%, respectively. This is attributed to the improved HTC of the hybrid nanofluid, which increased the heat removal from the PV cells.
- About 21.61 W of low electrical power was recorded by the reference PV module; this was increased to 24.41 W when cooling with DI water and 31.6 W when cooling with a mono nanofluid. The electrical power was later raised to 39.71 W by improving the hybrid nanofluid's thermal characteristics, which also boosted the HTC and improved the PV cells' ability to remove heat.
- The electrical efficiency of the PV/T system increased by 38.36% and thermal efficiency increased by 35.15% when a cooling approach using mono nanofluid with a concentration of 0.3 vol% was employed. The PV/T system's electrical and thermal efficiency have increased by 49.52% and 38.83%, respectively, when the hybrid nanofluid at 0.3 vol% is added in place of the DI water.
- Dispersing of $TiO_2$–$Fe_2O_3$ nanocomposite in the DI water has enhanced the *Nu* number and HTC by 42.72% and 23% higher than $TiO_2$ nanofluid positively improving the PV/T system performance. The pressure drop is increased using mono nanofluid by 83.16% compared to DI water and by 45.43% using $TiO_2$–$Fe_2O_3$ compared with the $TiO_2$ nanofluid. The increased density of nanofluid is undesirable that impacts the fluid circulation in tubes and pressure drop due to the increase of nanomaterials volume fraction.
- The PV/T system's thermal exergy efficiency was compromised, leading to a lower thermal exergy than electrical exergy, as a result of the fluid's outlet temperatures converging towards ambient temperature. In comparison to mono nanofluids at 0.3 vol%, hybrid nanofluids improve thermal and electrical energy efficiency by 63.81% and 49.4%, respectively, when utilized for cooling. The greater surface area and thermal properties of the hybrid nanomaterials enabled them to reduce the PV cells' temperature and increase the system's overall energy efficiency.
- In comparison to the reference PV module, the use of DI water, mono, and hybrid nanofluid for cooling at volume fraction of 0.3 vol% reduced exergy losses by 7.31%, 19.11%, and 56.14%, respectively. On the other hand, entropy generation decreased by 12% when DI water cooling was added. Additionally, the usage of mono and hybrid nanofluids at 0.3 vol% reduced the generation of entropy by 26.38% and 86.29%, respectively.
- Compared with previous studies, mono and hybrid nanofluids proposed in the current study had achieved better energy and exergy efficiency than many studies that used similar or different nanofluids. The adopted hybrid nanofluid achieved a better payback period than the mono nanofluid by 54 days and 160 days compared to the reference PV module.

## 5. Limitation and future work

This study involves a thermodynamic examination of the impact of mono and hybrid nanofluids on the energy and exergy of a PV/T system. Additionally, it examines the viability of using synthesised nanomaterials as cooling fluids in terms of their payback period. Only limited studies have evaluated the energy and exergy, which identify the irreversibility of the system and its effect by decreasing the exergy losses of the PV/T system. The results mentioned in the current study are limited to the specified period and cannot be considered to investigate the lifetime of this technology. This cooling technique may be viable for small-scale installations comprising of photovoltaic modules designed for a specific purpose. In the future, we intend to conduct a numerical study to demonstrate its
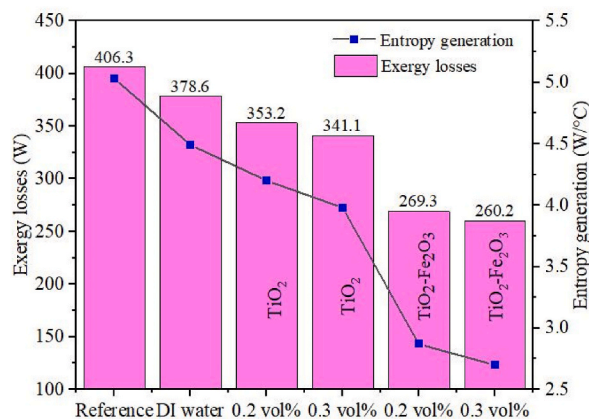
**Fig. 11.** Effect of volume fraction on energy losses and entropy generation.

potential for large-scale application, taking into account its cost. This will involve conducting more extensive experimental periods with the aid of numerical tools. Regarding nanofluids, it can adopt new hybrid nanofluids with new thermophysical properties with more stability that help improve heat exchange between PV/T system layers and reduce the PV cell's temperature. On the other hand, new improvements can be made in the PV/T configuration, such as heat exchanger design (tube diameter, the distance between tubes, adding fins. absorb plate thick).

## Data availability

Data will be made available on request.

## CRediT authorship contribution statement

**Mohammed Alktranee:** Conceptualization, Data curation, Formal analysis, Investigation, Methodology, Visualization, Writing – original draft, Writing – review & editing. **Mohammed Ahmed Shehab:** Formal analysis, Methodology, Visualization, Writing – original draft, Writing – review & editing, Investigation. **Zoltán Németh:** Formal analysis, Investigation, Supervision, Writing – review & editing. **Péter Bencs:** Data curation, Supervision, Validation, Visualization. **Klara Hernadi:** Investigation, Visualization, Writing – original draft, Writing – review & editing.

## Declaration of competing interest

The authors declare that they have no known competing financial interests or personal relationships that could have appeared to influence the work reported in this paper.

## Acknowledgements

## References

[1] N. Kannan, D. Vakeesan, Solar energy for future world:-A review, Renew. Sustain. Energy Rev. 62 (2016) 1092–1105.
[2] H. Al-Lami, N.N. Al-Mayyahi, Q. Al-Yasiri, R. Ali, A. Alshara, Performance enhancement of photovoltaic module using finned phase change material panel: an experimental study under Iraq hot climate conditions, Energy Sources, Part A Recovery, Util. Environ. Eff. 44 (3) (2022) 6886–6897.
[3] N.A.S. Elminshawy, D.G. El-Damhogi, I.A. Ibrahim, A. Elminshawy, A. Osama, Assessment of floating photovoltaic productivity with fins-assisted passive cooling, Appl. Energy 325 (2022), 119810.
[4] A.F. Abed, D.M. Hachim, S.E. Najim, A novel hybrid PV/T system for sustainable production of distillate water from the cooling of the PV module, in: IOP Conference Series: Materials Science and Engineering, IOP Publishing, 2021, 12049.
[5] A. Kasaeian, Y. Khanjari, S. Golzari, O. Mahian, S. Wongwises, Effects of forced convection on the performance of a photovoltaic thermal system: an experimental study, Exp. Therm. Fluid Sci. 85 (2017) 13–21.
[6] S. Aberoumand, S. Ghamari, B. Shabani, Energy and exergy analysis of a photovoltaic thermal (PV/T) system using nanofluids: an experimental study, Sol. Energy 165 (January) (2018) 167–177, https://doi.org/10.1016/j.solener.2018.03.028.
[7] P. Martínez-Merino, P. Estellé, R. Alcántara, I. Carrillo-Berdugo, J. Navas, Thermal performance of nanofluids based on tungsten disulphide nanosheets as heat transfer fluids in parabolic trough solar collectors, Sol. Energy Mater. Sol. Cell. 247 (2022), 111937.
[8] A.K. Hamzat, A.Z. Sahin, M.I. Omisanya, L.M. Alhems, Advances in PV and PV/T cooling technologies: a review, Sustain. Energy Technol. Assessments 47 (June) (2021) 101360, https://doi.org/10.1016/j.seta.2021.101360.

[9] N. Abdollahi, M. Rahimi, Potential of water natural circulation coupled with nano-enhanced PCM for PV module cooling, Renew. Energy 147 (2020) 302–309.

[10] Z. Arifin, S. Suyitno, D.D.D.P. Tjahjana, W.E. Juwana, M.R.A. Putra, A.R. Prabowo, The effect of heat sink properties on solar cell cooling systems, Appl. Sci. 10 (21) (2020) 7919.

[11] M. Alktranee, B. Péter, Energy and exergy analysis for photovoltaic modules cooled by evaporative cooling techniques, Energy Rep. 9 (2023) 122–132.

[12] M.O. Lari, A.Z. Sahin, Design, performance and economic analysis of a nanofluid-based photovoltaic/thermal system for residential applications, Energy Convers. Manag. 149 (2017) 467–484.

[13] N. Hooshmandzade, A. Motevali, S.R.M. Seyedi, P. Biparva, Influence of single and hybrid water-based nanofluids on performance of microgrid photovoltaic/thermal system, Appl. Energy 304 (2021), 117769.

[14] I. Karaaslan, T. Menlik, Numerical study of a photovoltaic thermal (PV/T) system using mono and hybrid nanofluid, Sol. Energy 224 (2021) 1260–1270.

[15] M. Hissouf, M. Najim, A. Charef, Numerical study of a covered Photovoltaic-Thermal Collector (PV/T) enhancement using nanofluids, Sol. Energy 199 (2020) 115–127.

[16] G.S. Menon, S. Murali, J. Elias, D.S.A. Delfiya, P. V Alfiya, M.P. Samuel, Experimental investigations on unglazed photovoltaic-thermal (PV/T) system using water and nanofluid cooling medium, Renew. Energy 188 (2022) 986–996.

[17] Z. Fu, et al., Experimental investigation on the enhanced performance of a solar PV/T system using micro-encapsulated PCMs, Energy 228 (2021), 120509.

[18] M. Alktranee, M.A. Shehab, Z. Németh, P. Bencs, K. Hernadi, Effect of zirconium oxide nanofluid on the behaviour of photovoltaic–thermal system: an experimental study, Energy Rep. 9 (2023) 1265–1277.

[19] A. Shahsavar, P. Jha, M. Arici, G. Kefayati, A comparative experimental investigation of energetic and exergetic performances of water/magnetite nanofluid-based photovoltaic/thermal system equipped with finned and unfinned collectors, Energy 220 (2021), 119714.

[20] A. Shahsavar, P. Jha, M. Arıcı, P. Estellé, Experimental investigation of the usability of the rifled serpentine tube to improve energy and exergy performances of a nanofluid-based photovoltaic/thermal system, Renew. Energy 170 (2021) 410–425.

[21] M.A. Shehab, et al., Preparation and photocatalytic performance of TiO$_2$ nanowire-based self-supported hybrid membranes, Molecules 27 (9) (2022) 2951.

[22] Y. Wang, J. Zhang, Ultrafine TiO2 (B) nanowires for ultrahigh-rate lithium-ion batteries, Ionics 26 (3) (2020) 1159–1164.

[23] M. Sołtys-Mróz, K. Syrek, J. Pierzchała, E. Wiercigroch, K. Malek, G.D. Sulka, Band gap engineering of nanotubular Fe$_2$O$_3$-TiO$_2$ photoanodes by wet impregnation, Appl. Surf. Sci. 517 (2020), 146195.

[24] M. Hosseinzadeh, M. Sardarabadi, M. Passandideh-Fard, Energy and exergy analysis of nanofluid based photovoltaic thermal system integrated with phase change material, Energy 147 (Mar. 2018) 636–647, https://doi.org/10.1016/j.energy.2018.01.073.

[25] M. Chandrasekar, T. Senthilkumar, Passive thermal regulation of flat PV modules by coupling the mechanisms of evaporative and fin cooling, Heat Mass Transfer/Waerme- und Stoffuebertragung 52 (7) (2016) 1381–1391, https://doi.org/10.1007/s00231-015-1661-9.

[26] Y. Yu, E. Long, X. Chen, H. Yang, Testing and modelling an unglazed photovoltaic thermal collector for application in Sichuan Basin, Appl. Energy 242 (2019) 931–941.

[27] F. Yazdanifard, M. Ameri, E. Ebrahimnia-Bajestan, Performance of nanofluid-based photovoltaic/thermal systems: a review, Renew. Sustain. Energy Rev. 76 (2017) 323–352.

[28] N.S.B. Rukman, A. Fudholi, N.F.M. Razali, M.H. Ruslan, K. Sopian, Energy and exergy analyses of photovoltaic-thermal (PV/T) system with TiO2/water nanofluid flow, in: IOP Conference Series: Earth and Environmental Science, IOP Publishing, 2019, 12075.

[29] A.H.A. Al-Waeli, M.T. Chaichan, H.A. Kazem, K. Sopian, J. Safaei, Numerical study on the effect of operating nanofluids of photovoltaic thermal system (PV/T) on the convective heat transfer, Case Stud. Therm. Eng. 12 (2018) 405–413.

[30] A.M. Hussein, R.A. Bakar, K. Kadirgama, K. V Sharma, Experimental measurement of nanofluids thermal properties, Int. J. Automot. Mech. Eng. 7 (2013) 850.

[31] Z. Qiu, X. Zhao, P. Li, X. Zhang, S. Ali, J. Tan, Theoretical investigation of the energy performance of a novel MPCM (Microencapsulated Phase Change Material) slurry based PV/T module, Energy 87 (2015) 686–698.

[32] M. Firoozzadeh, A.H. Shiravi, M. Lotfi, S. Aidarova, A. Sharipova, Optimum concentration of carbon black aqueous nanofluid as coolant of photovoltaic modules: a case study, Energy 225 (2021), https://doi.org/10.1016/j.energy.2021.120219.

[33] Y. Demirel, Thermodynamic analysis, Arabian J. Sci. Eng. 38 (2) (2013) 221–249.

[34] S.R. Maadi, A. Kolahan, M. Passandideh-Fard, M. Sardarabadi, R. Moloudi, Characterization of PV/T systems equipped with nanofluids-based collector from entropy generation, Energy Convers. Manag. 150 (August) (2017) 515–531, https://doi.org/10.1016/j.enconman.2017.08.039.

[35] O.R. Alomar, O.M. Ali, Energy and exergy analysis of hybrid photovoltaic thermal solar system under climatic condition of North Iraq, Case Stud. Therm. Eng. 28 (May) (2021), 101429, https://doi.org/10.1016/j.csite.2021.101429.

[36] A. Fudholi, et al., Energy and exergy analyses of photovoltaic thermal collector with∇-groove, Sol. Energy 159 (2018) 742–750.

[37] M. Sardarabadi, M. Hosseinzadeh, A. Kazemian, M. Passandideh-Fard, Experimental investigation of the effects of using metal-oxides/water nanofluids on a photovoltaic thermal system (PV/T) from energy and exergy viewpoints, Energy 138 (2017) 682–695, https://doi.org/10.1016/j.energy.2017.07.046.

[38] T.T. Chow, G. Pei, K.F. Fong, Z. Lin, A.L.S. Chan, J. Ji, Energy and exergy analysis of photovoltaic-thermal collector with and without glass cover, Appl. Energy 86 (3) (2009) 310–316, https://doi.org/10.1016/j.apenergy.2008.04.016.

[39] A. Farzanehnia, M. Sardarabadi, Exergy in photovoltaic/thermal nanofluid-based collector systems, in: Exergy and its Application-Toward Green Energy Production and Sustainable Environment, IntechOpen, 2019.

[40] B.C. Pak, Y.I. Cho, Hydrodynamic and heat transfer study of dispersed fluids with submicron metallic oxide particles, Exp. Heat Transfer Int. J. 11 (2) (1998) 151–170.

[41] W. Yu, S.U.S. Choi, The role of interfacial layers in the enhanced thermal conductivity of nanofluids: a renovated Maxwell model, J. Nanoparticle Res. 5 (1) (2003) 167–171.

[42] Y. Xuan, W. Roetzel, Conceptions for heat transfer correlation of nanofluids, Int. J. Heat Mass Tran. 43 (19) (2000) 3701–3707.

[43] H.C. Brinkman, The viscosity of concentrated suspensions and solutions, J. Chem. Phys. 20 (4) (1952) 571.

[44] F. Abbas, et al., Towards convective heat transfer optimization in aluminum tube automotive radiators: potential assessment of novel Fe2O3-TiO2/water hybrid nanofluid, J. Taiwan Inst. Chem. Eng. 124 (2021) 424–436.

[45] E.B. Öğüt, Natural convection of water-based nanofluids in an inclined enclosure with a heat source, Int. J. Therm. Sci. 48 (11) (2009) 2063–2073.

[46] J.J. Michael, S. Iniyan, Performance analysis of a copper sheet laminated photovoltaic thermal collector using copper oxide–water nanofluid, Sol. Energy 119 (2015) 439–451.

[47] D.C. Jordan, S.R. Kurtz, K. VanSant, J. Newmiller, Compendium of photovoltaic degradation rates, Prog. Photovoltaics Res. Appl. 24 (7) (2016) 978–989.

[48] P. Pounraj, et al., Experimental investigation on Peltier based hybrid PV/T active solar still for enhancing the overall performance, Energy Convers. Manag. 168 (2018) 371–381.

[49] M. Chandrasekar, S. Rajkumar, D. Valavan, A review on the thermal regulation techniques for non integrated flat PV modules mounted on building top, Energy Build. 86 (2015) 692–697.

[50] T.K. Murtadha, A.A. dil Hussein, A.A.H. Alalwany, S.S. Alrwashdeh, M. Ala'a, Improving the cooling performance of photovoltaic panels by using two passes circulation of titanium dioxide nanofluid, Case Stud. Therm. Eng. 36 (2022), 102191.

[51] H. Adun, et al., Synthesis and application of ternary nanofluid for photovoltaic-thermal system: comparative analysis of energy and exergy performance with single and hybrid nanofluids, Energies 14 (15) (2021) 4434.

[52] I. Wole-Osho, H. Adun, M. Adedeji, E.C. Okonkwo, D. Kavaz, M. Dagbasi, Effect of hybrid nanofluids mixture ratio on the performance of a photovoltaic thermal collector, Int. J. Energy Res. 44 (11) (2020) 9064–9081.

[53] R. Sathyamurthy, A.E. Kabeel, A. Chamkha, A. Karthick, A. Muthu Manokar, M.G. Sumithra, Experimental investigation on cooling the photovoltaic panel using hybrid nanofluids, Appl. Nanosci. 11 (2) (2021) 363–374.

[54] A. Shahsavar, Experimental investigation of thermal and electrical performances of a nanofluid-cooled photovoltaic/thermal system equipped with a sheet-and-grooved serpentine tube collector, Energy Eng. Manag. 12 (1) (2023) 120–129, https://doi.org/10.22052/12.1.120.

[55] Z. Khalili, M. Sheikholeslami, L. Momayez, Hybrid nanofluid flow within cooling tube of photovoltaic-thermoelectric solar unit, Sci. Rep. 13 (1) (2023), https://doi.org/10.1038/s41598-023-35428-6.

[56] M.T. Chaichan, et al., Optimizing MWCNT-based nanofluids for photovoltaic/thermal cooling through preparation parameters, ACS Omega (2022), https://doi.org/10.1021/acsomega.2c07226.

[57] M. Alktranee, M. Ahmed Shehab, Z. Németh, P. Bencs, K. Hernadi, Experimental study for improving photovoltaic thermal system performance using hybrid titanium oxide-copper oxide nanofluid, Arab. J. Chem. 16 (9) (Sep. 2023), 105102, https://doi.org/10.1016/j.arabjc.2023.105102.

[58] M. Sardarabadi, M. Passandideh-Fard, S.Z. Heris, Experimental investigation of the effects of silica/water nanofluid on PV/T (photovoltaic thermal units), Energy 66 (2014) 264–272.

[59] M. Alktranee, M.A. Shehab, Z. Németh, P. Bencs, K. Hernadi, T. Koós, Energy and exergy assessment of photovoltaic-thermal system using tungsten trioxide nanofluid: an experimental study, Int. J. Thermofluids (2022), 100228.

[60] M. Sardarabadi, M. Hosseinzadeh, A. Kazemian, M. Passandideh-Fard, Experimental investigation of the effects of using metal-oxides/water nanofluids on a photovoltaic thermal system (PV/T) from energy and exergy viewpoints, Energy 138 (2017) 682–695.